Editors' Suggestion

Hybrid Photonic-Plasmonic Cavity Design for Very Large Purcell Factors at Telecommunication Wavelengths

Angela Barreda,[1,2,*] Laura Mercadé,[3,4] Mario Zapata-Herrera,[5] Javier Aizpurua,[5,6] and Alejandro Martínez[3]

[1] *Friedrich Schiller University Jena, Institute of Solid State Physics, Helmholtzweg 3, Jena 07743, Germany*
[2] *Friedrich Schiller University Jena, Institute of Applied Physics, Abbe Center of Photonics, Albert-Einstein-Str. 15, Jena 07745, Germany*
[3] *Nanophotonics Technology Center, Universitat Politècnica de València, Camino de Vera s/n, Valencia 46022, Spain*
[4] *Departament d'Enginyeria Electrónica i Biomédica, Facultat de Física, Universitat de Barcelona*
[5] *Centro de Física de Materiales, Centro Mixto CSIC-UPV/EHU, P. Manuel de Lardizabal 5, 20018 San Sebastián/Donostia, Basque Country, Spain*
[6] *Donostia International Physics Center, P. Manuel de Lardizabal 4, 20018 San Sebastián/Donostia, Basque Country, Spain*

(Received 11 April 2022; revised 18 July 2022; accepted 9 September 2022; published 27 October 2022)

Hybrid photonic-plasmonic cavities can be tailored to display high Q factors and extremely small mode volumes simultaneously, which ultimately results in large values of the Purcell factor, F_P. Amongst the different hybrid configurations, those based on a nanoparticle-on-a-mirror plasmonic cavity provide one of the lowest mode volumes, though so far their operation has been constrained to wavelengths below 1 μm. Here, we propose a hybrid configuration consisting of a silicon photonic crystal cavity with a slot at its center in which a gold nanoparticle is introduced. This hybrid system operates at telecom wavelengths and provides high Q-factor values ($Q \approx 10^5$) and small normalized mode volumes ($V_m \approx 10^{-4}$), leading to extremely large Purcell-factor values, $F_P \approx 10^7 - 10^8$. The proposed cavity could be used in different applications such as molecular optomechanics, bio- and chemosensing, efficient quantum emitters, or enhanced Raman spectroscopy in the relevant telecom-wavelength regime.

DOI: 10.1103/PhysRevApplied.18.044066

I. INTRODUCTION

The local density of optical states (LDOS) quantifies the available number of electromagnetic states that can be occupied by a photon in a certain position of a system. A high local value of the LDOS will result in enhanced light-matter interaction at that location. In this way, the environment of an emitter can be tailored to maximize the LDOS using, e.g., optical cavities. At resonance, the LDOS gives us the Purcell factor, F_P, which originally accounted for the enhancement of the spontaneous emission of an atom in a cavity [1–3]. By definition, the Purcell factor is proportional to the ratio between the Q factor and the mode volume V_m, as [4,5]:

$$F_P = \frac{3}{4\pi^2}\frac{Q}{V_m}, \tag{1}$$

where V_m is the mode volume normalized by the wavelength (λ) over the local refractive index (n) cubed $(\lambda/n)^3$ and Q is the quality factor. Note that Eq. (1) requires that the line width of the emitter is narrower than the line width of the optical resonance, which is satisfied in most cases. This suggests a route to designing photonic systems that exhibit simultaneously a high Q factor and an ultrasmall V_m to maximize F_P and enhance light-matter interaction.

Dielectric cavities can greatly enhance the Purcell factor, since they can have large Q-factor values as a result of the negligible absorption loss [6]. However, the diffraction limit usually prevents them from achieving subwavelength-scale mode volumes, so $V_m \approx 1$ unless special "slotted" configurations are used [7–9]. On the contrary, plasmonic cavities formed by metallic nanoparticles (NPs) can overcome the diffraction limit, leading to ultrasmall V_m values[10]. However, Joule losses in the metal reduce the reachable Q factor to values $Q \approx 10$ [11,12].

In the past few years, hybrid photonic-plasmonic cavities have been introduced as systems providing large F_p, as they can potentially combine the best of both worlds: high Q-factor values due to the dielectric photonic cavity and small mode volumes as a result of the metallic NP

*angela.barreda@uni-jena.de

[11,13–22]. Indeed, by modifying the coupling between the photonic and plasmonic modes, the Q factor and V_m can be tuned between the values of the bare NP and the cavity [17]. Different configurations of hybrid photonic-plasmonic cavities have been suggested so far. Some of the most attractive ones consist of a bow-tie nanoantenna placed on a dielectric photonic crystal nanobeam cavity operating at transverse-electric (TE) polarization [17] ($F_p \approx 1 \times 10^4$). The main limitation of this configuration is that the plasmonic gap has to be defined lithographically, reaching minimum values of several nanometers, which prevents reaching the nanometer-scale (and below) gaps that leads to extreme plasmonic localization [23–25].

Nanoparticle-on-a-mirror (NPoM) cavities are far superior for achieving the smallest possible mode volumes, as plasmonic gaps around 1 nm and below can be created. The reason is that NPs can be deposited on top of self-assembled monolayers (SAMs) formed on metallic surfaces, so that the plasmonic gap widths equal the SAM thickness [26–30]. Recently, a hybrid system combining a NPoM configuration with GaP photonic crystal cavities—operating under transverse-magnetic (TM) polarization at visible wavelengths—has been introduced [31]. Due to the NPoM-based design, nanometer- and subnanometer-scale plasmonic gaps can potentially be achieved and combined with relatively large Q factors. By means of this hybrid system, the Purcell factor is enhanced by one order of magnitude with respect to hybrid configurations based on bow-tie nanoantennas ($F_p \approx 1 \times 10^5$) [31].

Most of the previous work on hybrid photonic cavities has been focused on the visible-wavelength range, due to the huge interest in enhancing light-matter interaction in that spectral region [17]. However, their realization at telecom wavelengths ($\lambda \approx 1550$ nm) is also highly interesting, for several reasons: first, because of the multiple available applications (mostly related to high-speed optical communications and data processing but also recently label-free biosensing) as well as advanced available equipment (laser, amplifiers, and high-speed photodetectors); and, second, because of the emergence of the silicon photonics area, which has become the standard technology for the production of large-volume photonic integrated circuits. In this regard, enhancing the Purcell factor improves the performance of single-photon sources enormously [17], so hybrid cavities could play a role in building such sources at telecom wavelengths, progress on which has been quite elusive so far [32]. By locating the quantum emitter in the gap between the metallic nanoparticle and the cavity sidewall, it would be possible to accelerate its emission process [33]. Importantly, the realization of efficient quantum sources at telecom wavelengths would enable the transmission of quantum information through widely deployed fiber-based optical communication networks. In laser applications, which in our approach could be realized by embedding proper emitters in the slot, large Purcell-factor values would decrease the lasing threshold power, which is proportional to V_m/Q [34]. In the case of biosensing, silicon photonics provides a route for manufacturing low-cost chips for highly sensitive label-free detection in an aqueous environment [35]. The use of cavities with large Q and small V_m should lead to extreme sensitivity (down to the single molecule level) and a large reduction of the footprint (in comparison, e.g., to biosensors based on ring resonators [36]). Although the figure of merit is not directly the Purcell factor [17], nonlinear processing could also benefit from large Q/low V_m cavities. For instance, hybrid cavities could greatly reduce switching powers and footprints in nonlinear all-optical switches on silicon [37,38]. Also, hybrid cavities could provide a route for efficient Raman spectroscopy in silicon chips, which should make use of telecom wavelengths to avoid silicon absorption below 1.1 μm [39].

There have been many demonstrations of silicon cavities operating at telecom wavelengths with Q factors over 10^4 using lithographically defined one-dimensional (1D) ($F_p \approx 2.7 \times 10^6$) [40] or two-dimensional (2D) ($F_p \approx 1.7 \times 10^5$) [41] photonic crystal cavities while showing $V_m \approx 1$. Reaching $V_m < 1$ becomes feasible by defining thin slots in silicon and taking advantage of the discontinuities of the normal electric field [7,42] but with the minimum slot size being limited by lithography. In a previous work [8], complex subwavelength structuring of silicon (down to approximately 10 nm) has also enabled $V_m < 2 \times 10^{-4}$ to be reached.

Hybrid systems have also recently been proposed in silicon technology for telecom wavelengths. In Ref. [19], a hybrid photonic-plasmonic nanocavity, constituted by an L3 photonic crystal nanocavity and a plasmonic bow-tie nanoantenna, has been shown to have an ultrahigh figure of merit Q/V of 8.4×10^6 $(\lambda/n)^{-3}$ ($F_p \approx 6.3 \times 10^5$). However, either in the silicon-only cavity [8] or in the hybrid approach [19], the extreme field localization enabled by the NPoM cavity has still been missing.

In this work, we propose a hybrid photonic-plasmonic cavity that combines silicon and the NPoM approach to obtain extreme field localization and large Q at resonance. This hybrid consists of a silicon photonic cavity with a slot at its center [9,42], operating at TE polarization at telecom wavelengths, and a gold NP, which is located at the cavity of the slot. The NP can potentially be separated from the silicon walls of the slot by a SAM, thus reaching the nanometer- and even subnanometer-scale localized fields at resonance. Our design achieves $Q \approx 1 \times 10^5$ and $V_m \approx 1 \times 10^{-4}$, giving rise to Purcell-factor values of $F_P \approx 1 \times 10^7$–$1 \times 10^8$, which are 2–3 orders of magnitude larger than those reported previously, based on NPoM cavities combined with photonic crystals, and 2 orders of magnitude larger than those corresponding to hybrid photonic-plasmonic cavities operating at

telecom wavelengths. This is mainly due to the nanoscale confinement provided by the slot-nanoparticle combination and the radiation suppression resulting from the photonic crystal structure. By combining top-down and bottom-up approaches, we also suggest a route to fabricating the hybrid cavity, which may be used to improve the performance of current silicon photonic devices as well as to envisage applications in the relevant telecom-wavelength domain.

II. DESCRIPTION OF THE HYBRID CAVITY

Figure 1 depicts the proposed hybrid photonic-plasmonic configuration. A gold NP is located at the center of the slot of a 1D silicon photonic crystal cavity operating under TE polarization at telecom wavelengths. The distance between the NP and the photonic crystal wall (the gap, d) is $d = 1$ nm, which approximately models the thickness of a SAM. The silicon wall behaves here as the mirror, though showing lower reflectance than a metallic one. Such a small gap, which is not defined lithographically but by carefully placing the NP in the cavity spaced by a SAM, should allow for extreme light confinement, thus giving rise to small V_m. Separately, the bare dielectric cavity, i.e., without the NP, provides high Q-factor values due to the excitation of a defect mode within the band gap of the photonic crystal. When the metallic NP is located in the gap, the scattering pathways of the NP dipolar response will be strongly suppressed as a result of the photonic band gap of the dielectric cavity, leading to high Q factors for the hybrid system (Q_{Hyb}). In addition, due to the presence of the NP, the mode volume of the dielectric cavity will be decreased by squeezing the field in the gap region, leading to ultrasmall V_m of the hybrid system (V_{Hyb}). So, the small V_{Hyb} together with the high Q_{Hyb} should result in LDOS values that are not attainable by the bare components (NP or dielectric cavity alone), as we show in Sec. IV. In order to understand which parameters prevent further increase of the Q-factor, we draw on the analytical coupled oscillator model introduced in Ref. [17], where it has been shown how the properties of the bare dielectric cavity and NP limit the possible Q_{Hyb} and V_{Hyb} that can be attained [17]. It has been demonstrated that the Q factor of the hybrid system (Q_{Hyb}) is determined not only by the losses introduced by the metallic NP but also by the detuning between the NP and the cavity, the cavity (V_c) and the NP (V_{NP}) mode volumes, and the Q factor of the bare cavity (Q_c). In the particular case of considering gaps as small as 1 nm, the Q factor is mainly hampered by absorption due to the small distance between the emitter and the metallic particle, as we show in Sec. IV.

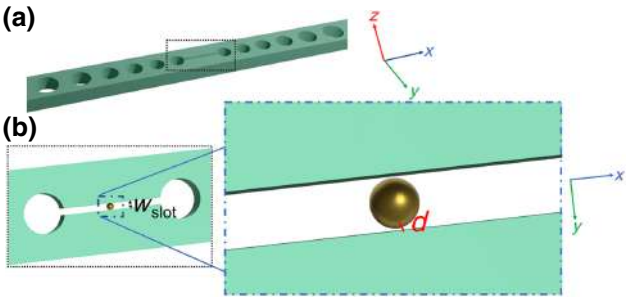

FIG. 1. Schematics of the proposed system. (a) Geometry of the 1D slotted photonic crystal cavity. (b) A top view of the center of the cavity, where the slot of width w can be distinguished. A gold spherical NP is located inside the slot. The distance between the NP and the cavity wall in the y direction is $d = 1$ nm, as shown in the close-up view and marked with a dashed-dotted line.

It is worth remarking that although placing the right material in the nanometer-scale gap is not so obvious, it could be done for many applications in a relatively easy way. For instance, many useful materials can form SAMs that can be attached to the target surface. Although many SAMs bind mainly to gold (see, e.g., Refs. [43,44]), other SAMs can be designed to bind to silicon (see, e.g., Ref. [45]). Once the SAM is attached to the mirror, the NP could be deposited on it by several methods. For single emitters or quantum dots, it may be more complicated but more and more techniques are under development to couple atoms or molecules to waveguides and cavities (see, e.g., Ref. [46]).

III. METHODS

The eigenfrequencies and LDOS calculations shown in this work are obtained by means of the finite-element method (FEM), implemented in the COMSOL MULTIPHYSICS commercial software [47]. In particular, the radio-frequency (rf) module is used. The optical constants for the gold NP are taken from Ref. [48]. The refractive index for silicon is considered to be $n = 3.48$. To attain the LDOS, the structure is illuminated by an electric point-dipole source, the dipole moment of which is considered along the y axis (i.e., along the axis connecting the sphere and the cavity). The normalized LDOS is defined as

$$\mathrm{LDOS} = \frac{P_{\mathrm{rad}} + P_{\mathrm{no-rad}}}{P_{\mathrm{radvacuum}}}, \tag{2}$$

where P_{rad} is the radiative power density and $P_{\mathrm{no-rad}}$ is the power-loss density. The numerator corresponds to the radiative and nonradiative power emitted by the dipole coupled to the structure. However, the denominator contains the radiative power emitted by the dipole in a vacuum. The dipole is located at the center of the structure and in the middle of the gap between the NP and the silicon-slot sidewalls. Experimentally, this spacer would be filled by a suitable SAM. For computational purposes, the hybrid geometry is surrounded by a cylindrical air region of radius 9μm. An additional smaller cylinder with

a radius of 5 μm and made of air is placed in the center of the larger cylinder. The scattered power (P_{rad}) is calculated at the boundaries of the smaller cylinder, whereas the nonradiative power density is obtained by means of the volume integration of the losses in the metallic NP. The dipole source is surrounded by a sphere with a diameter that is equal to the gap size ($d = 1$ nm) to ensure a sufficiently fine grid in close proximity to the dipole source. The mesh of the surrounding air medium is chosen to be smaller than 600 nm. The mesh of the gold sphere is smaller than 6 nm. The chosen sizes for the mesh of the slot, the cavity surrounding the slot, and the holes and cavity surrounding the holes are smaller than 15 nm, 22.5 nm, 45 nm, and 52.5 nm, respectively. The mesh of the sphere surrounding the dipole source is smaller than 0.2 nm. The cylindrical region of air is surrounded by a perfectly matched layer (PML) with a thickness of 3 μm. The near-field plots at the eigenfrequencies of interest are attained with the eigenmode solver of COMSOL Multiphysics. The same mesh is used for the LDOS and eigenmode calculations and for the different analyzed structures: the dielectric (no NP) and hybrid cavity. In all cases, the same geometry is considered and only the optical constants of the materials (if present or not) are changed appropriately.

Note that a local description of the dielectric response is properly adopted in our calculations, as nonlocal effects [49] can be disregarded in our system due to the large size of the nanoparticle considered, as well as to the absence of any small metal-insulator-metal (M-I-M) gap [50,51].

IV. RESULTS

A. Photonic band diagram

The 1D silicon photonic crystal cavity consists of a silicon waveguide of width $h = 550$ nm and thickness $t = 220$ nm patterned with holes and with a slot in the defect section, as depicted in Fig. 1(a). The beam is drilled with a set of circular holes to produce a TE band gap around $\lambda = 1550$ nm. Figure 2(a) shows the TE-like band diagram when the holes are spaced by a distance $a = 580$ nm and have a radius $r = 0.365a$, showing a wide band gap (shadowed region) as expected. To build the cavity, we include two photonic crystal mirrors with the previous dimensions at each side of the cavity while the period is adiabatically reduced from $a = 580$ nm down to $a = 331.5$ nm (while keeping the r/a ratio constant) when moving toward the cavity center. This allows us to blue shift the dielectric band and obtain a confined mode in the band gap, as depicted by the red dashed line in Fig. 2(a). Finally, a slot section of width $w = 40$ nm and length $l = 547$ nm is introduced between the central holes of the cavity to enhanced the TE field. Note that this slot width is achievable using standard silicon nanofabrication [9].

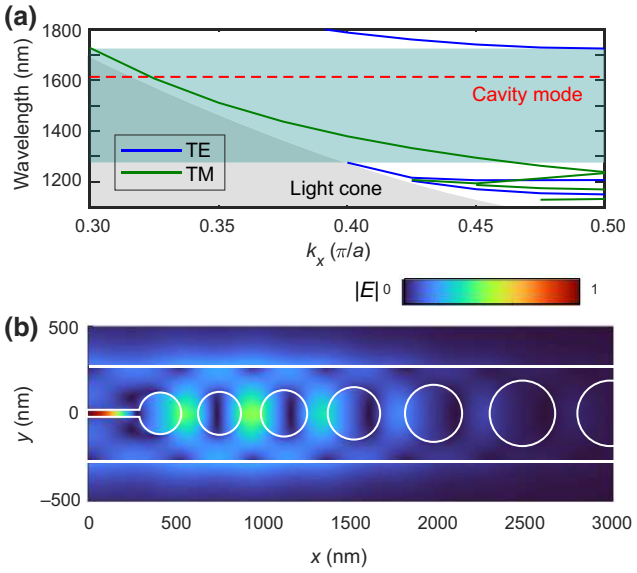

FIG. 2. (a) The photonic band diagram of the mirror unit cell. The TE-like (TM-like) bands are depicted in blue (green). The shadowed region corresponds to the TE-like quasi–band gap where the photonic crystal cavity mode confined in the middle region is located (depicted with a red dashed line). (b) The mode profile of the electric field amplitude $|E|$ (X-Y crosscut) normalized to its maximum value for the slotted photonic crystal cavity without the spherical gold NP.

The near-field map at the eigenfrequency of the confined mode ($\lambda = 1613$ nm) in the 1D photonic crystal cavity, following the previous design, is presented in Figure 2(b). It can clearly be seen that the electric field is well confined in the slot placed at the center of the cavity. It is worth mentioning that the cavity resonance is red shifted with respect to the gold NP resonance. In previous works, it has been shown that this condition is necessary to improve the performance of the hybrid cavity with respect to the isolated components [11,17,18].

B. Comparison of Q-V_m values for the bare cavity and the hybrid system

In Figs. 3(a) and 3(b), we present the calculated LDOS for the bare cavity (slot width $w = 40$ nm) and the hybrid system composed of the silicon cavity plus a gold NP of radius $R = 19$ nm, respectively. For the bare cavity, the Q factor is retrieved from fitting the LDOS to a Lorentzian function. Once the Q factor is known, the mode volume is recovered by the inversion of Eq. (1). The obtained Q factor of the bare cavity is $Q_c = 1.6 \times 10^5$, while the mode-volume value is $V_c = 4 \times 10^{-2}$. Note that while it is true that quasinormal modes (QNMs) are highly appropriate for studying hybrid structures such as the ones presented in this work [52], V_m can also be retrieved from the LDOS calculation, once the Q factor is known [17,18]. As expected, high Q values are achieved and they could

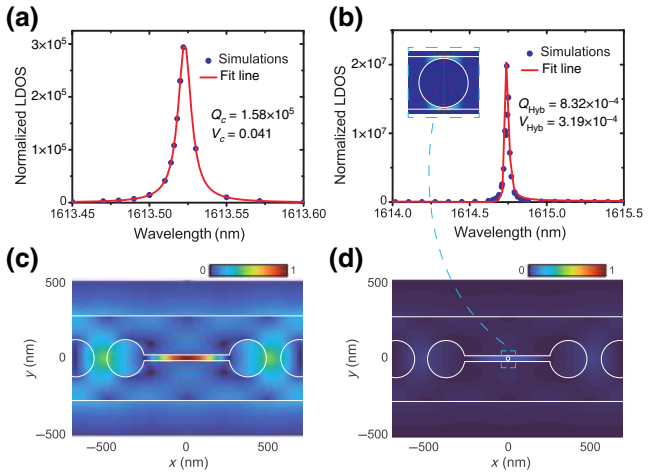

FIG. 3. The normalized LDOS, Q factor, and V_m for (a) the bare-silicon photonic crystal (Q_c, V_c) and (b) the hybrid plasmonic-photonic cavity (Q_{Hyb}, V_{Hyb}). The slot size is $w = 40$ nm and the radius of the gold NP is $R = 19$ nm. The mode profile of $|E|$ (X-Y crosscut) normalized to its maximum value in the slot for (c) the bare-silicon photonic crystal and (d) the hybrid photonic-plasmonic cavity. The inset in (b) shows a close-up view of the confined mode profile $|E|$ of the hybrid photonic-plasmonic cavity in the center of the cavity.

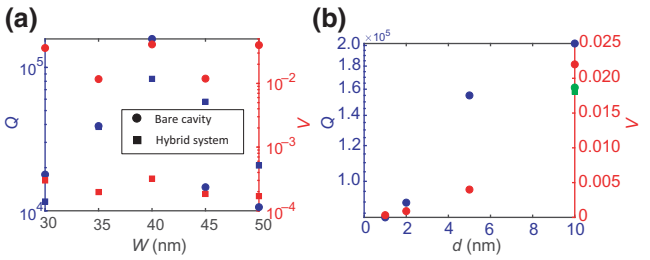

FIG. 4. (a) The Q-factor (blue markers) and V_m (red markers) values for the bare cavity (points) and the hybrid system (squares) as a function of the slot size w. The radius of the gold NP is varied accordingly to keep the gap distance between the NP and the wall of the photonic crystal to $d = 1$ nm. (b) The Q-factor (blue markers) and V_m (red markers) values for the hybrid system as a function of the gap size. The size of the slot is kept constant at $w = 40$ nm. The NP is located at the center of the gap. The green circle (square) represents the Q factor (V_m) for the hybrid system ($w = 40$ nm and $d = 10$ nm) when the NP is stuck to only one of the cavity sidewalls (asymmetric cavity).

even be higher given a more meticulous design of the bare cavity. However, V_m is still large in comparison to the values that can be obtained by considering metallic nanostructures ($V_{\mathrm{NP}} \approx 1 \times 10^{-6}$). When the NP is introduced in the gap, the Q factor of the hybrid system is only slightly diminished ($Q_{\mathrm{Hyb}} = 8.3 \times 10^4$) but there is a 2-orders-of-magnitude reduction of V_m down to $V_{\mathrm{Hyb}} = 3.2 \times 10^{-4}$ as a result of the hybridization of the metallic NP with the photonic cavity. For the hybrid cavity, a Fano fitting is necessary due to the hybridization of two different modes: the mode corresponding to the cavity and that of the NP.

If we observe the near-field maps of the electric field in the slot for the bare cavity and the hybrid system [see Figs. 3(c) and 3(d), respectively], we see that the gold NP squeezes the slot field into a nanometer-scale region, which is the purpose of introducing the NPoM approach. Therefore, the hybrid system provides a route to extreme localization of telecom-wavelength fields while keeping large Q values.

C. Evolution of Q-V_m values with the slot size

From an experimental point of view, some differences in the size of the slot can be expected with respect to the nominal parameters due to imperfections during the fabrication process. In this section, we analyze the influence of the slot width on the Q-factor and V_m values. Figure 4(a) shows the Q-factor and V_m values as a function of the slot size for the bare cavity and the hybrid system. We observe that as the size of the slot is modified (both increased or decreased) with respect to the optimum value $w = 40$ nm, the Q factor decreases by almost one order of magnitude. However, the V_m values are not so affected due to changes in w, especially for the bare cavity. In all cases, the gap distance between the gold NP and the cavity wall is $d = 1$ nm, which means that the NP radius is modified accordingly for each w value. As previously described, the Q factor of the hybrid system (Q_{Hyb}) can be similar to that of the bare cavity (Q_c) when the NP resonance is far detuned with respect to that of the cavity. In this case, the optimization of Q_c leads to larger values of Q_{Hyb}. Our design provides the highest Q_c for a slot size of $w = 40$ nm, as can be observed from the blue dots in Fig. 4(a). For that reason, the largest Q_{Hyb} is attained for $w = 40$ nm. Note also that the fact of having an optimum for a certain value of the slot width is related to the ability of the dielectric system (with the NP) to optimally confine the optical field in the slot region. In a similar system (a silicon-slot waveguide), there is an optimum of the slot width to maximize the confinement in the slot region, this behavior being comparable to that of our cavity [53].

D. Evolution of Q-V_m values with the NP-cavity gap

Small imperfections in the chemical production of the NP can also generate imprecision in its size, provoking uncertainty in the gap distance between the NP and the wall of the photonic cavity. To analyze this effect, in Fig. 4(b) we present the Q-factor and V_m values for different gap sizes for a slot cavity of $w = 40$ nm. In particular, the size of the NP is varied between $R = 19$ nm and $R = 10$ nm, leading to variations in the gap from $d = 1$ nm to $d = 10$ nm. As the gap increases, both Q_{Hyb} and V_{Hyb} increase. This effect is due to the lower confinement of the electromagnetic radiation in the gap.

Moreover, in a practical implementation, it would be difficult to perfectly fit the NP in the gap so that it gets stuck both lateral sidewalls. Instead, the most realistic scenario would be a NP smaller than the gap width and getting stuck to one of the SAMs by chemical interaction. We simulate this situation by considering a silicon cavity with a slot width of w = 40 nm, where a particle of $R = 10$ nm is introduced so that it is separated by 1 nm from one of the cavity sidewalls. We obtain $Q = 1.61 \times 10^5$ and $V_m = 0.018$, values quite similar to those obtained for the symmetry case. Therefore, the same conclusions can apply to the case of the asymmetric hybrid cavity.

V. CONCLUSIONS

In this work, we introduce a design of a hybrid photonic-plasmonic cavity, which combines a 1D silicon photonic cavity with a slot in its center, operating under TE polarization at telecom wavelengths, with a spherical gold NP located at the center of the slot. This configuration shows how to merge the NPoM approach with silicon photonic crystal cavities in order to achieve extreme light confinement in nanometer-scale gaps. Using this nanostructure, we obtain a hybrid mode showing Q-factor values larger than $Q_{\mathrm{Hyb}} = 1 \times 10^5$ and mode volumes smaller than $V_{\mathrm{Hyb}} = 1 \times 10^{-4}$. This gives rise to Purcell-factor values of $F_P \approx 1 \times 10^7$–$1 \times 10^8$, which are 2 or 3 orders of magnitude higher than those obtained in previous NPoM hybrid photonic-plasmonic cavities [31] or metallic bow-tie-antenna coupled photonic crystals operating under TE polarization [17]. If we extend the comparison to hybrid cavities operating at telecom wavelengths, we can conclude that our hybrid cavity provides Purcell factors 2 orders of magnitude larger than the hybrid photonic-plasmonic nanocavity reported in Ref. [19]. This is mainly due to the nanoscale confinement provided by the slot-nanoparticle combination and the radiation suppression resulting from the photonic crystal structure.

From a practical perspective, the 1D silicon photonic crystal cavity can be fabricated using standard silicon technology [8,9]. It is also possible to release the silicon beam from the substrate [54] as in the configuration in this work. NPs can be deposited later by drop casting, potentially falling into the slot, as recently demonstrated for plasmonic nanoslits [43]. The use of optical forces could even be used to efficiently trap the NPs inside the slot, as demonstrated in slot waveguides [55]. Moreover, some techniques would enable the transfer of isolated gold NPs to the slot, as recently demonstrated for other nanophotonics structures [56]. If the beam is not released from the substrate, the photonic band gap would be somewhat reduced but high-Q modes are still possible and the NPs could be deposited on the silica substrate at the slot bottom. Thus, we foresee that a combination of top-down (for the photonic crystal cavity) and bottom-up (for the deposition of the gold NPs) techniques would make the experimental realization of this cavity possible, enabling molecular-scale light confinement together with large Q factors.

The building of hybrid cavities that operate at telecom wavelengths not only offers perspectives in applications that already exist in that spectral regime (optical communications, photonic biosensing [35,57], and nonlinear signal processing) but could also enable the transfer of (near-) visible-regime applications (such as surface-enhanced Raman spectroscopy [58] or optomechanically driven frequency conversion [43,44]) to a domain where a huge amount of high-quality instrumentation (tunable lasers, high-speed photodetectors, and amplifiers) is available, while being implementable in silicon-compatible chips. Advances in optical communications will be made by enabling silicon-based lasers with a lower threshold due to the placement of quantum emitters in the cavity gap. This could also be used in future quantum networks, since the quantum emitter would be tuned at telecom wavelengths so that the generated quantum information could be transported via optical fibers throughout very long links. Regarding nonlinear processing, the squeezing of light in nanometer-scale volumes, while keeping a high Q factor, could be used in high-speed and low-power all-optical switches that employ Kerr-nonlinear media in the gap region through the use of silicon-compatible chips.

ACKNOWLEDGMENTS

A.B. is grateful for financial support by the Deutsche Forschungsgemeinschaft (DFG, German Research Foundation) through the International Research Training Group (IRTG) 2675 "Meta-ACTIVE," Project No. 437527638. L.M. is grateful for financial support from the Next Generation European Union program, Ministerio de Universidades (Gobierno de España). A.M. acknowledges funding from H2020 European Commission (THOR-H2020-EU-829067) and the Generalitat Valenciana (PROMETEO/2019/123). M.Z.H. and J.A. acknowledge the Spanish Ministry of Science (Project No. PID2019-107432GB-I00) for financial support and grant IT1526-22 for consolidated university groups of the Basque Government.

APPENDIX A: RADIATIVE AND NONRADIATIVE POWER CONTRIBUTIONS

It is important to consider the radiative efficiency in our system. We show that high values of the LDOS can be attained but these take into account both the radiative and nonradiative contributions. Figures 5(a), 5(c), 5(e), and 5(g) show the LDOS for different gaps between the gold NP and the cavity wall (slot size $w = 40$ nm). The ratio of the radiative to the nonradiative contribution for each case is presented in Figs. 5(b), 5(d), 5(f), and 5(h). From the obtained results, it can be concluded

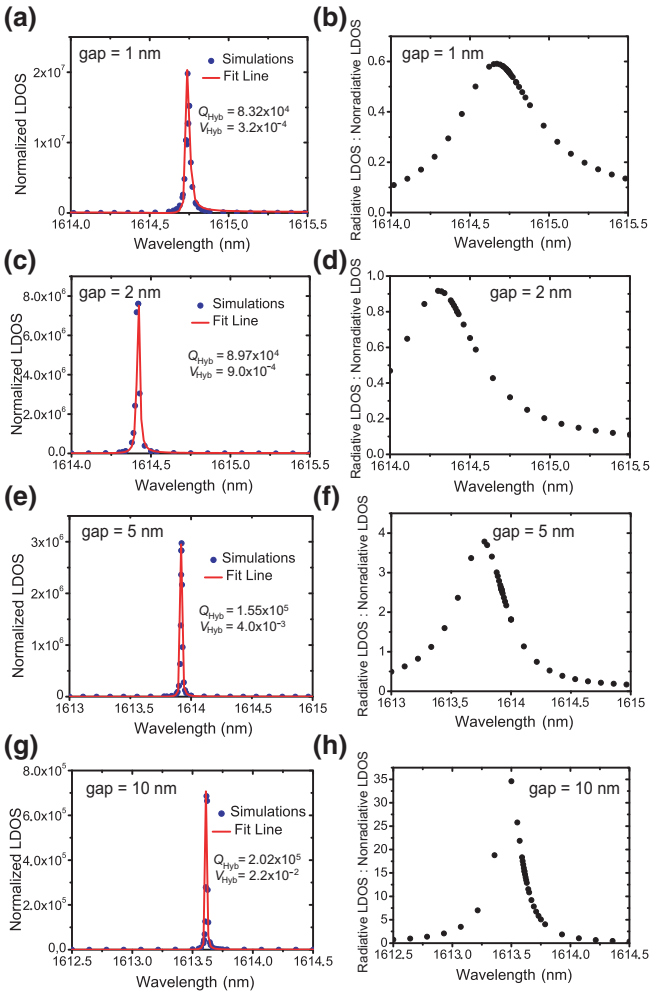

FIG. 5. The normalized LDOS for gap sizes (a) $d = 1$ nm, (c) $d = 2$ nm, (e) $d = 5$ nm, and (g) $d = 10$ nm, for the hybrid system. The size of the slot is kept constant at $w = 40$ nm. The ratio of the radiative to nonradiative LDOS for gap sizes (b) $d = 1$ nm, (d) $d = 2$ nm, (f) $d = 5$ nm, and (h) $d = 10$ nm, for the hybrid system.

that the LDOS decreases with the increase in the gap size. However, the opposite behavior is attained for the ratio of the radiative to the nonradiative LDOS. In this case, as the gap increases, the ratio also increases. In fact, for the smaller gap (1 nm), the emitter (dipole) is very close to the gold NP, instigating strong Ohmic losses. In this case, the nonradiative contribution is larger than the radiative one. For larger gaps (5 nm), the radiative contribution dominates over the nonradiative power. However, even for the worst case (gap = 1 nm), the ratio of the radiative and nonradiative contributions takes values larger than 0.6.

APPENDIX B: PURCELL FACTOR

The Purcell factor measures the LDOS at resonance. The LDOS can be expressed in terms of the Green's function tensor $\overleftrightarrow{\mathbf{G}}$ [59].

Considering a two-level quantum emitter located at position $\mathbf{r}_0$ and weakly coupled to an antenna, its decay rate, according to Fermi's Golden Rule, is given by

$$\Gamma = \frac{\pi\omega}{3\hbar\epsilon_0}|\langle g|\hat{\mathbf{p}}|e\rangle|^2\boldsymbol{\rho}_{\mathbf{p}}(\mathbf{r}_0,\omega), \tag{B1}$$

where $\langle g|\hat{\mathbf{p}}|e\rangle$ is the transition dipole moment between the excited state $|e\rangle$ and the ground state $|g\rangle$ of the emitter, ω is the transition frequency, $\hbar$ is the reduced Planck's constant, ϵ_0 is the vacuum dielectric permittivity, and $\boldsymbol{\rho}_{\mathbf{p}}$ corresponds to the projected LDOS, which is expressed as

$$\boldsymbol{\rho}_{\mathbf{p}}(\mathbf{r}_0,\omega) = \frac{6\omega}{\pi c^2}[\mathbf{n}_p \cdot \mathrm{Im}\{\overleftrightarrow{\mathbf{G}}(\mathbf{r}_0,\mathbf{r}_0,\omega)\}\cdot\mathbf{n}_p], \tag{B2}$$

where $\mathbf{n}_p$ is a unit vector along the direction of the dipole $\mathbf{p}$.

The previous expressions correspond to a quantum mechanical description. However, the Purcell factor can also be expressed in classical terms by replacing the two-level transition by its corresponding dipole moment $\mathbf{p}$ [59].

The power dissipated by the classical dipole is related to the Green's function by

$$P = \frac{\pi\omega^2}{12\epsilon_0}|\mathbf{p}|^2\boldsymbol{\rho}_{\mathbf{p}}(\mathbf{r}_0,\omega). \tag{B3}$$

The ratio between the emission rate of the dipole in the presence and in the absence of the antenna is known as the Purcell factor:

$$\frac{P}{P^0} = \boldsymbol{\rho}_{\mathbf{p}}(\mathbf{r}_0,\omega)\frac{\pi^2c^3}{\omega^2}, \tag{B4}$$

where P^0 is given by

$$P^0 = \frac{|\mathbf{p}|^2\omega^4}{12\pi\epsilon_0 c^3}, \tag{B5}$$

in which c is the speed of light in vacuum.

It has been shown that the Purcell factor (for the case of emission through a single channel) can be expressed as

$$F_P = \frac{3}{4\pi^2}\frac{Q}{V_m}, \tag{B6}$$

where Q corresponds to the quality factor and V_m is the effective mode volume expressed in units of wavelength (λ) cubed in the medium of interest of refractive index n.

[1] E. M. Purcell, Spontaneous emission probabilities at radio frequencies, Phys. Rev. **69**, 681 (1946).

[2] A. F. Koenderink, On the use of Purcell factors for plasmon antennas, Opt. Lett. **35**, 4208 (2010).

[3] X. Zambrana-Puyalto and N. Bonod, Purcell factor of spherical Mie resonators, Phys. Rev. B **91**, 195422 (2015).

[4] L. Novotny and B. Hecht, *Principles of Nano-Optics* (New York: Cambridge University Press, New York, 2012), 2nd ed.

[5] R. Sprik, B. A. van Tiggelen, and A. Lagendijk, Optical emission in periodic dielectrics, Europhys. Lett. **35**, 265 (1996).

[6] J. T. Choy, B. J. M. Hausmann, T. M. Babinec, I. Bulu, M. Khan, P. Maletinsky, A. Yacoby, and M. Lonĉar, Enhanced single-photon emission from a diamond-silver aperture, Nat. Photon. **5**, 738 (2011).

[7] H. Choi, M. Heuck, and D. Englund, Self-Similar Nanocavity Design with Ultrasmall Mode Volume for Single-Photon Nonlinearities, Phys. Rev. Lett. **118**, 223605 (2017).

[8] S. Hu, M. Khater, R. Salas-Montiel, E. Kratschmer, S. Engelmann, W. M. J. Green, and S. M. Weiss, Experimental realization of deep-subwavelength confinement in dielectric optical resonators, Sci. Adv. **4**, eaat2355 (2018).

[9] P. Seidler, K. Lister, U. Drechsler, J. Hofrichter, and T. Stöferle, Slotted photonic crystal nanobeam cavity with an ultrahigh quality factor-to-mode volume ratio, Opt. Express **21**, 32468 (2013).

[10] S. A. Maier, *Plasmonics: Fundamentals and Applications* (Springer, New York, 2007).

[11] H. M. Doeleman, E. Verhagen, and A. F. Koenderink, Antenna-cavity hybrids: Matching polar opposites for Purcell enhancements at any linewidth, ACS Photonics **3**, 1943 (2016).

[12] G. M. Akselrod, C. Argyropoulos, T. B. Hoang, C. Ciracì, C. Fang, J. Huang, D. R. Smith, and M. H. Mikkelsen, Probing the mechanisms of large Purcell enhancement in plasmonic nanoantennas, Nat. Photon. **8**, 835 (2014).

[13] I. Mukherjee, G. Hajisalem, and R. Gordon, One-step integration of metal nanoparticle in photonic crystal nanobeam cavity, Opt. Express **19**, 22462 (2011).

[14] M. Kamandar Dezfouli, R. Gordon, and S. Hughes, Modal theory of modified spontaneous emission of a quantum emitter in a hybrid plasmonic photonic-crystal cavity system, Phys. Rev. A **95**, 013846 (2017).

[15] I. Mukherjee and R. Gordon, Analysis of hybrid plasmonic-photonic crystal structures using perturbation theory, Opt. Express **20**, 16992 (2012).

[16] M. K. Dezfouli, R. Gordon, and S. Hughes, Molecular optomechanics in the anharmonic cavity-QED regime using hybrid metal–dielectric cavity modes, ACS Photonics **6**, 1400 (2019).

[17] I. M. Palstra, H. M. Doeleman, and A. F. Koenderink, Hybrid cavity-antenna systems for quantum optics outside the cryostat?, Nanophotonics **8**, 1513 (2019).

[18] H. M. Doeleman, C. D. Dieleman, C. Mennes, B. Ehler, and A. F. Koenderink, Observation of cooperative Purcell enhancements in antenna-cavity hybrids, ACS Nano **14**, 12027 (2020).

[19] H. Zhang, Y.-C. Liu, C. Wang, N. Zhang, and C. Lu, Hybrid photonic-plasmonic nano-cavity with ultra-high Q/V, Opt. Lett. **45**, 4794 (2020).

[20] E. Arbabi, S. M. Kamali, S. Arnold, and L. L. Goddard, Hybrid whispering gallery mode/plasmonic chain ring resonators for biosensing, Appl. Phys. Lett. **105**, 231107 (2014).

[21] Y. Hong, W. Ahn, S. V. Boriskina, X. Zhao, and B. M. Reinhard, Directed assembly of optoplasmonic hybrid materials with tunable photonic-plasmonic properties, J. Phys. Chem. Lett. **6**, 2056 (2015).

[22] C. Klusmann, R. N. S. Suryadharma, J. Oppermann, C. Rockstuhl, and H. Kalt, Hybridizing whispering gallery modes and plasmonic resonances in a photonic metadevice for biosensing applications, J. Opt. Soc. Am. B **34**, D46 (2017).

[23] N. A. Hatab, C.-H. Hsueh, A. L. Gaddis, S. T. Retterer, J.-H. Li, G. Eres, Z. Zhang, and B. Gu, Free-standing optical gold bowtie nanoantenna with variable gap size for enhanced Raman spectroscopy, Nano Lett. **10**, 4952 (2010).

[24] W. Zhu and K. B. Crozier, Quantum mechanical limit to plasmonic enhancement as observed by surface-enhanced Raman scattering, Nat. Commun. **5**, 5228 (2014).

[25] H. Duan, A. I. Fernández-Domínguez, M. Bosman, S. A. Maier, and J. K. W. Yang, Nanoplasmonics: Classical down to the nanometer scale, Nano Lett. **12**, 1683 (2012).

[26] G. Lévêque and O. J. F. Martin, Optical interactions in a plasmonic particle coupled to a metallic film, Opt. Express **14**, 9971 (2006).

[27] C. Ciracì, R. T. Hill, J. J. Mock, Y. Urzhumov, A. I. Fernández-Domínguez, S. A. Maier, J. B. Pendry, A. Chilkoti, and D. R. Smith, Probing the ultimate limits of plasmonic enhancement, Science **337**, 1072 (2012).

[28] J. J. Baumberg, J. Aizpurua, M. H. Mikkelsen, and D. R. Smith, Extreme nanophotonics from ultrathin metallic gaps, Nat. Mater. **18**, 668 (2019).

[29] C. Carnegie, J. Griffiths, B. de Nijs, C. Readman, R. Chikkaraddy, W. M. Deacon, Y. Zhang, I. Szabó, E. Rosta, J. Aizpurua, and J. J. Baumberg, Room-temperature optical picocavities below 1 nm^3 accessing single-atom geometries, J. Phys. Chem. Lett. **9**, 7146 (2018).

[30] M. Barbry, P. Koval, F. Marchesin, R. Esteban, A. G. Borisov, J. Aizpurua, and D. Sánchez-Portal, Atomistic near-field nanoplasmonics: Reaching atomic-scale resolution in nanooptics, Nano Lett. **15**, 3410 (2015).

[31] A. I. Barreda, M. Zapata-Herrera, I. M. Palstra, L. Mercadé, J. Aizpurua, A. F. Koenderink, and A. Martínez, Hybrid photonic-plasmonic cavities based on the nanoparticle-on-a-mirror configuration, Photon. Res. **9**, 2398 (2021).

[32] H. Zhao, M. T. Pettes, Y. Zheng, and H. Htoon, Site-controlled telecom-wavelength single-photon emitters in atomically-thin $MoTe_2$, Nat. Commun. **12**, 6753 (2021).

[33] A. Barreda, S. Hell, M. Weissflog, A. Minovich, T. Pertsch, and I. Staude, Metal, dielectric and hybrid nanoantennas for enhancing the emission of single quantum dots: A comparative study, Quant. Spectrosc. Radiat. Transf. **276**, 107900 (2021).

[34] M. T. Hill and M. C. Gather, Advances in small lasers, Nat. Photonics **8**, 908 (2014).

[35] F. Vollmer and S. Arnold, Whispering-gallery-mode biosensing: Label-free detection down to single molecules, Nat. Methods **5**, 591 (2008).

[36] L. Castelló-Pedrero, M. I. Gómez-Gómez, J. García-Rupérez, A. Griol, and A. Martínez, Performance improvement of a silicon nitride ring resonator biosensor operated in the TM mode at 1310 nm, Biomed. Opt. Express **12**, 7244 (2021).

[37] J. Leuthold, C. Koos, and W. Freude, Nonlinear silicon photonics, Nat. Photonics **4**, 535 (2010).

[38] A. Martínez, J. Blasco, P. Sanchis, J. V. Galán, J. García-Rupérez, E. Jordana, P. Gautier, Y. Lebour, S. Hernández, R. Spano, R. Guider, N. Daldosso, B. Garrido, J. M. Fedeli, L. Pavesi, and J. Martí, Ultrafast all-optical switching in a silicon-nanocrystal-based silicon slot waveguide at telecom wavelengths, Nano. Lett. **10**, 1506 (2010).

[39] A. Dhakal, A. Raza, F. Peyskens, A. Z. Subramanian, S. Clemmen, N. L. Thomas, and R. Baets, Efficiency of evanescent excitation and collection of spontaneous Raman scattering near high index contrast channel waveguides, Opt. Express **23**, 27391 (2015).

[40] P. B. Deotare, M. W. McCutcheon, I. W. Frank, M. Khan, and M. Lončar, High quality factor photonic crystal nanobeam cavities, Appl. Phys. Lett. **94**, 121106 (2009).

[41] Y. Akahane, T. Asano, B.-S. Song, and S. Noda, High-q photonic nanocavity in a two-dimensional photonic crystal, Nature **425**, 944 (2003).

[42] J. T. Robinson, C. Manolatou, L. Chen, and M. Lipson, Ultrasmall Mode Volumes in Dielectric Optical Microcavities, Phys. Rev. Lett. **95**, 143901 (2005).

[43] W. Chen, P. Roelli, H. Hu, S. Verlekar, S. P. Amirtharaj, A. I. Barreda, T. J. Kippenberg, M. Kovylina, E. Verhagen, A. Martínez, and C. Galland, Continuous-wave frequency upconversion with a molecular optomechanical nanocavity, Science **374**, 1264 (2021).

[44] A. Xomalis, X. Zheng, R. Chikkaraddy, Z. Koczor-Benda, E. Miele, E. Rosta, G. A. E. Vandenbosch, A. Martínez, and J. J. Baumberg, Detecting mid-infrared light by molecular frequency upconversion in dual-wavelength nanoantennas, Science **374**, 1268 (2021).

[45] I. Bakish, V. Artel, T. Ilovitsh, M. Shubely, Y. Ben-Ezra, A. Zadok, and C. N. Sukenik, Self-assembled monolayer assisted bonding of Si and InP, Opt. Mater. Express **2**, 1141 (2012).

[46] P. Lodahl, S. Mahmoodian, S. Stobbe, A. Rauschenbeutel, P. Schneeweiss, J. Volz, H. Pichler, and P. Zoller, Chiral quantum optics, Nature **541**, 473 (2017).

[47] COMSOL MULTIPHYSICS 5.0, (COMSOL Inc., 2015), https://www.comsol.com.

[48] E. D. Palik, *Handbook of Optical Constants of Solids* (Academic Press, Orlando, 1998).

[49] Y. Yang, D. Zhu, W. Yan, A. Agarwal, M. Zheng, J. D. Joannopoulos, P. Lalanne, T. Christensen, K. K. Berggren, and M. Soljaĉić, A general theoretical and experimental framework for nanoscale electromagnetism, Nature **576**, 248 (2019).

[50] W. Zhu, R. Esteban, A. G. Borisov, J. J. Baumberg, P. Nordlander, H. J. Lezec, J. Aizpurua, and K. B. Crozier, Quantum mechanical effects in plasmonic structures with subnanometre gaps, Nat. Commun. **7**, 11495 (2016).

[51] T. V. Teperik, P. Nordlander, J. Aizpurua, and A. G. Borisov, Robust Subnanometric Plasmon Ruler by Rescaling of the Nonlocal Optical Response, Phys. Rev. Lett. **110**, 263901 (2013).

[52] P. Lalanne, W. Yan, K. Vynck, C. Sauvan, and J.-P. Hugonin, Light interaction with photonic and plasmonic resonances, Laser Photonics Rev. **12**, 1700113 (2018).

[53] P. Sanchis, J. Blasco, A. Martínez, and J. Martí, Design of silicon-based slot waveguide configurations for optimum nonlinear performance, J. Lightwave Technol. **25**, 1298 (2007).

[54] L. Mercadé, L. L. Martín, A. Griol, D. Navarro-Urrios, and A. Martínez, Microwave oscillator and frequency comb in a silicon optomechanical cavity with a full phononic bandgap, Nanophotonics **9**, 3535 (2020).

[55] A. H. J. Yang, S. D. Moore, B. S. Schmidt, M. Klug, M. Lipson, and D. Erickson, Optical manipulation of nanoparticles and biomolecules in sub-wavelength slot waveguides, Nature **457**, 71 (2009).

[56] J. Redolat, *et al.*, In preparation.

[57] F. De Angelis, M. Patrini, G. Das, I. Maksymov, M. Galli, L. Businaro, L. C. Andreani, and E. Di Fabrizio, A hybrid plasmonic-photonic nanodevice for label-free detection of a few molecules, Nano Lett. **8**, 2321 (2008).

[58] J. Losada, A. Raza, S. Clemmen, A. Serrano, A. Griol, R. Baets, and A. Martínez, Sers detection via individual bowtie nanoantennas integrated in Si_3N_4 waveguides, IEEE J. Sel. Top. Quantum Electron. **25**, 1 (2019).

[59] P. Bharadwaj, B. Deutsch, and L. Novotny, Optical antennas, Adv. Opt. Photon. **1**, 438 (2009).